Crystal texture-dependent magnetic and magnetotransportproperties of Fe_3O_4 films grown on oxidized Si substrates by reactive deposition

V.V. Balashev,[1,2*]K.S. Ermakov,[1]A.Yu. Samardak,[1]A.V. Ognev,[1]A.S. Samardak,[1,5]S.V. Komogortsev, [3,6] M.N. Volochaev,[3,4] A.S. Tarasov,[3,6]V.V.Korobtsov[1,2]

[1]*School of Natural Sciences, Far Eastern Federal University, Vladivostok, Russia*

[2]*Institute of Automation and Control Processes, FEB RAS, Vladivostok, Russia*

[3]*Kirensky Institute of Physics, SB RAS, Krasnoyarsk, Russia*

[4]*Siberian State Aerospace University, Krasnoyarsk, Russia*

[5]*National Research South Ural State University, Chelyabinsk, Russia*

[6]*Siberian Federal University, Krasnoyarsk, Russia*

Email: balashev@mail.dvo.ru

Abstract

Nanocrystalline magnetite (Fe_3O_4) films with various preferred crystallite orientation were grown on oxidized silicon surface by reactive iron deposition in an oxygen atmosphere. Depending on the partial pressure of oxygen (O_2), the evolution of the structural, magnetic, and magnetotransport properties of the grown films was investigated. From data analysis, it was found that the growth of films containing only the Fe_3O_4 phase occurs in a certain O_2 pressure range, and the magnetite crystallites may have (311) or (110) preferential orientation. From the transmission electron microscopy data, it was found that films with (311) and (110) textures have a column structure. An increase in the O_2 pressure leads to a transition from the growth of a film with the (311) texture to a film with the (110) one having larger Fe_3O_4 crystallites. A film with the (110) texture showed both higher valuesof saturation magnetization and magnetoresistance. The analysis of approach to magnetic saturation revealed that local magnetic anisotropy of the crystallites in textured films is much higher than the anisotropy of bulk magnetite due to the large surface contribution. The approach to magnetization saturation in combination with the FORC diagram method proved the existence of the exchange coupling between large and small grains.

Introduction

Magnetic and transport properties of magnetite nanoparticles and thin films grown on various substrates have attracted undiverted attention of researchers over the past two decades[1-9]. Magnetite is a promising candidate for spintronics due to the theoretically predicted 100% spin polarization of conduction electrons [10], which is much larger than the experimentally defined values [1,4,11]. In turn, the growth of magnetite films on a silicon substrate is interesting, becausethere is the possibility of the spin-polarized electronsinjection from a ferromagnet into a semiconductor[12,13]. The synthesis of magnetite films is often implemented by methods such as pulse laser deposition (PLD) [14-16]and magnetron sputtering[2,17,18], using an oxygen inlet into the growth chamber during the sputtering of iron or iron oxide from the target. However, it should be noted that the level of the oxygen partial

pressure during the growth process may affect the magnetic and electrical properties of the grown Fe_3O_4 films. Thus, the authors of [19] recently showed that this can be attributed to a change in the ratio of ionsFe^{3+}/Fe^{2+} in the inverse spinel lattice of an epitaxial magnetite film. In the case of polycrystalline films, from an analysis of Raman spectroscopy data, it was found that the partial pressure of oxygen affects the density of antiphase domain boundaries (APBs) [20], as well as the size of crystallites of Fe_3O_4.

The iron oxide films prepared by authors of various works differ in thickness and experimental conditions under which they were grown, which makes it difficult to compare the data. At the same time, it can be said that low oxygen pressure leads to the growth of films with a high iron content[2,21,22], for which magnetic hysteresis loops are characterized by high saturation magnetization (M_s) and low coercive force (H_c). The authors note that a further increase in the oxygen pressure leads to the growth of films in which the M_s and H_c values become comparable for bulk Fe_3O_4. Since, in a certain range of oxygen pressure, the formation of the Fe_3O_4 phase occurs predominantly, a detailed study of the properties of the magnetite films as a function of pressure is very interesting. We have found [23] that, with some pressure variation, a preferred orientation of crystallites appears in the polycrystalline Fe_3O_4 film. This structural change depending on the oxygen pressure was also observed in X-ray spectra[2,24]. Lai et al [24] showed that ion beam deposition (IBD) of magnetite is accompanied by the appearance of the intense (100) peak on the XRD spectrum, and then its attenuation and amplification of the (311) peak with a subsequent increase in oxygen pressure. The Fe_3O_4 films deposited by magnetron sputtering [2] had (110), (100) and (111) preferred orientations as a function of pressure. With the exception of the aforementioned works, there is no complete information about the relationship between the structural, magnetic, and electrical properties of polycrystalline Fe_3O_4 films grown at different oxygen pressures. In this work, we have grown magnetite films with different preferredorientation of Fe_3O_4 crystallites using reactive deposition of iron in an oxygen atmosphere. The influence of the structure on the magnetic and magnetotransport properties of the films is studied and discussed in details.

Experimental details

The magnetite films were grown in an ultrahigh-vacuum setup “Katun” equipped with reflection high-energy electron diffraction system (RHEED, Omicron RH20S) and spectral ellipsometry. Base pressure did not exceed 10^{-10}Torr. Monocrystalline silicon wafers ($0.5 \times 10 \times 20$ mm^3) of n-type (7.5 Ω·cm) with orientation (001) were used as substrates. Before loading the substrates into the vacuum chamber, the cleaning of their surface, as well as the formation of a thin SiO_2 layer (1.5nm) on it, was carried out in the same way as in [25]. After loading into the vacuum chamber, samples were preheated at 500°C for 1 hour.

Magnetite films of 75 nm nominal thickness were grown on the SiO_2/Si(001) surface by reactive deposition of Fe in an O_2 atmosphere at a substrate temperature of 300°C. Iron was deposited at a rate of 2.5 nm/min by thermal evaporation from the Knudsen cell with an alumina crucible (Al_2O_3). Taking into account crystal structure of $Fe_3O_4$and Fe, the amount of deposited Fe needed to form a magnetite film with a thickness of 75 nm was approximately half of the film thickness — 37 nm. The films were grown at the following oxygen partial pressures: $1\cdot10^{-6}$Torr, $1.5\cdot10^{-6}$Torr, $3\cdot10^{-6}$Torrand $7\cdot10^{-6}$Torr.

The RHEED patterns were recorded in the process of film deposition at the electron beam glancing angles to the surface ~0.5-1°. After unloading of the samples from the vacuum chamber, the structure of the films was investigated using transmission electron microscope (TEM HT-7700, Hitachi).The X-ray diffraction (XRD) probing of the magnetite films was carried out on a Bruker D8 Advance X-ray diffractometer (CuKα radiation, 1.54184 Å), in the point-by-point scanning mode. The maximum deviation of the positions of reflections determined using NIST SRM 1976 was less than 0.01° in 2θ. The crystallite size (D_{cr}) was calculated according to the Scherrer equation $D_{cr} = \frac{k\lambda}{\beta}\cos\theta$, where k is the shape factor (0.9 used here), λ is the X-ray wavelength used, β is the full peak broadening (width)

at half maximum intensity (FWHM), after subtracting the instrumental line broadening, in radiansand θ is the Bragg diffraction peak angle. This calculation supplements the analysis of TEM images of the thin films.

Studies of the electrical and magnetic properties of the films were carried out at room temperature after unloading samples from the ultrahigh vacuum chamber. Magnetic hysteresis loops were obtained by an induction method using a vibrating sample magnetometer (Lake Shore VSM 7410). The resistivity and magnetoresistancemeasurements of iron oxide films were carried out using a 4-probe method on samples of 4×4 mm^2using a measuring module that is part of VSM. A magnetic field was applied along the film plane (along the line of contact arrangement) in the range of ± 10 kOe.

Results and discussion

1. Crystal structure characterization

As seen from Fig. 1(a), after deposition of Fe at low oxygen pressure P_{O2} ~$1\cdot10^{-6}$Torr, the RHEEDpattern from the surface shows Debye rings and their radii characterizethe diffraction from the polycrystalline Fe_3O_4 film. Uniform distribution of the intensity along the rings points to random orientationof the grains in the Fe_3O_4film. As seen from the TEM image of the film, its thickness is t~ 45nm, not 75nm as was expected for magnetitestructure. The average grain height corresponds to the thickness of this film, and the lateral dimensions are 33 ± 6nm. The small thickness of the iron oxide film can be explained by the incomplete oxidation of Fe, which is directly confirmed by the absence of the more intensive (311) peak of Fe_3O_4, Fig.1(e). Moreover, there is an indirect confirmation based on the observation of diffusion rings from wustite (FeO) at the initial stage of growth [23]. The observed diffractionrings from magnetite after deposition are associated with the transmission diffraction of electronsin the more oxidized surface layer of the film(grains) consisting of magnetite.

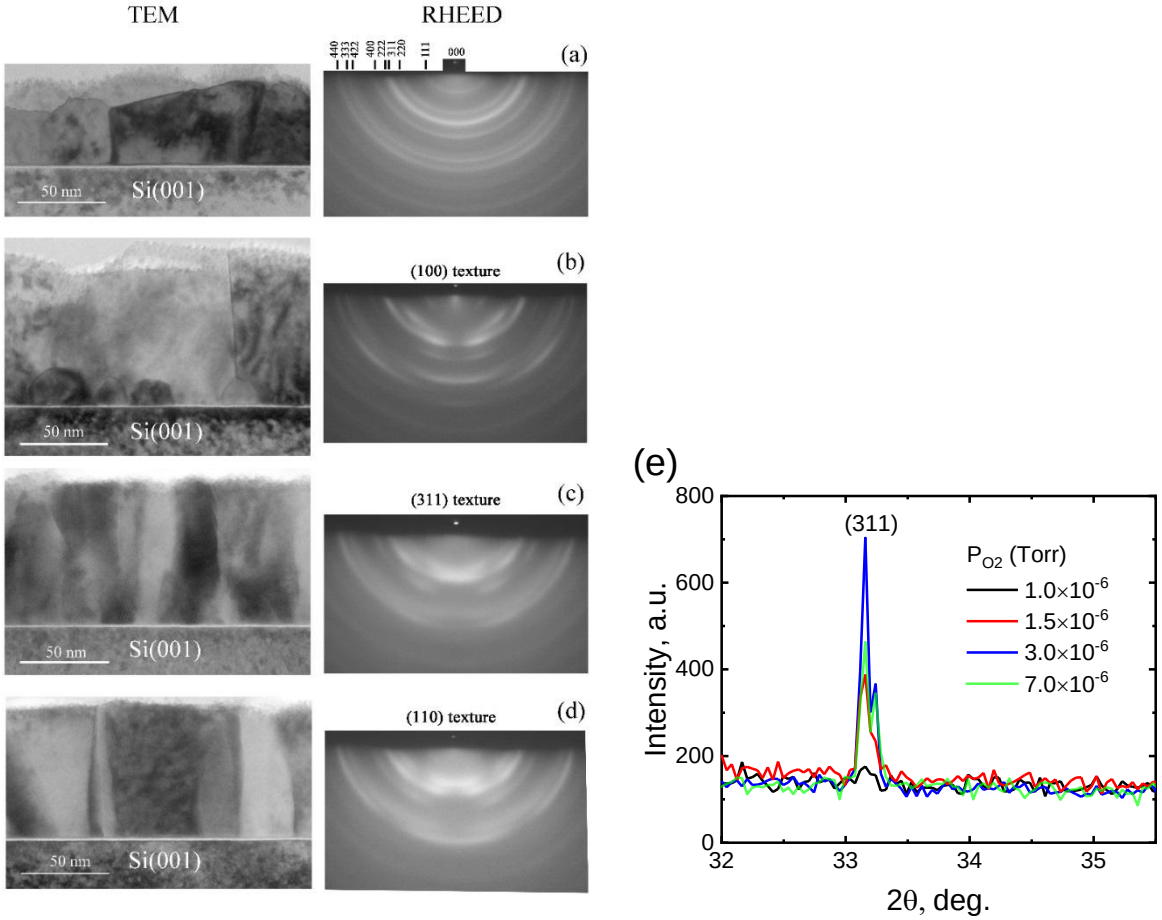

Fig.1 TEM images and RHEED patterns of Fe_3O_4 films grown at different P_{O2}: (a) $1\cdot10^{-6}$Torr, (b) $1.5\cdot10^{-6}$Torr, (c) $3\cdot10^{-6}$Torr and (d) $7\cdot10^{-6}$Torr. (e) Shortcut XRD spectra for the Fe_3O_4 filmsgrown at different P_{O2}.

After the deposition of Fe at P_{O2} ~ $1.5 \cdot 10^{-6}$Torr, in the RHEED pattern, instead of continuous rings, arcs were observed, which are characteristic of a Fe_3O_4 film with a texture (Fig. 1(b)). The observedRHEED pattern agrees well with the theoretical one for (100)texture, the axis of which is normal to the surface [25]. It can be seen from the TEM image that the film contains both coarse grains with a height of ~ 75 nm and lateral size of ~ 55 ± 11 nm, as well as small grains located at the interface with the SiO_2layer. If at the initial stage of growth we observed a superposition of arcs and continuous rings in the RHEED pattern, then with an increase in the film thickness, there was a complete transition to broken rings consisting of arcs. It can be assumed that at the initial stage of growth, grains are formed with both random and preferred (100) orientation. The transition to the RHEED pattern, consisting only of arcs from (100) texture, indicates a higher growth rate of grains with (100) orientation. We associate large grains in the TEM image with grains that have a preferred(100) orientation, and small ones, at the interface, with grains with a random orientation. It is interesting to note that in the case of IBD [24] an increase in pressure/flow of O_2 to a certain value led to an increase in the Fe_3O_4 phase fraction, which was characterized by an intense (400) peak on the XRD spectrum. It is possible that, as in the present work, the Fe_3O_4 film had the (100) texture.

As seen from the TEM image in Fig.1(c), the Fe_3O_4 film grown at $P_{O2}=3 \cdot 10^{-6}$ Torr has a columnar structure. The height of the largest grains is comparable to the film thickness of 75 nm, while their lateral dimensions (22 ± 3 nm) are approximately threetimes smaller. Obviously, that these grains have the predominant (311) orientation found from the analysis of the RHEED pattern for this film [23] and confirmed by the XRD study, Fig.1(e). Film growth at this O_2 pressure occurs according to the competitive mode[26], in which the grain growth in the direction normal to the(311) lattice plane goes faster. The observed transition from (100) to (311) texture was alsofound in the aforementioned work [24], in which an increase in the oxygen flow led to a complete decay in the intensity of the (400) peak and an increase in the (311) peak.

The magnetite film grown at a higher pressure,$P_{O2}=7 \cdot 10^{-6}$ Torr (Fig. 1(d)), also has a columnar structure and consists mainly of large grains. Lateral grain sizes increase by ~ 2 timescompare with the previous filmand reach 49 ± 5 nm. According to the analysis of the RHEED pattern[23], this film has the (110) texture. It is assumed that an increase in the O_2 pressure leads to an increase in the diffusion mobility of the adsorbates on {110} faces that have less free energy than the {311} faces. As a result, lateral growth of grains oriented by the corresponding faces parallel to the substrate surfaceoccurs. In this case the film is formed by coalescence [26], rather than the competitive mode of growth. An increase in the lateral size of the grains with O_2 pressure, detected from the TEM data, can serve as confirmation of this assumption.

As seen in Fig.1(e), all samples deposited at $P_{O2} \geq 1.5 \cdot 10^{-6}$ Torr have the (311) peak in the XRD pattern, which is the main indicator of a Fe_3O_4 phase existence. It is worth to note, that in bulk monocrystalline magnetite the (311) peak is situated at $2\theta=35.423^{\circ}$. However, deposition of Fe on a Si substrate induces the tensile stresses in the thin iron oxide films, which are the main reason for the (311) peak's shift on 2.264º towards smaller angles. This crystal structure transformation increases the interplanar distance in magnetite from 2.534 Å up to 2.702 Å.

Magnetite films grown at low temperatures did not have a texture, and the grain size was several times smaller.In the case of deposition at temperatureof ~ 37°Cusing the same deposition method [27], the preferredorientation of the grains of the Fe_3O_4 film was not observed. The author of the work notes that the phase composition of the film fully corresponded to magnetite at a pressure of $P_{O2}=5 \cdot 10^{-6}$ Torr. In the case of polycrystalline magnetite films grown at room temperature by magnetron sputtering with thickness of 60nm [28] and 70nm [29], the grains had no preferred orientation as well, and their size was 12-13 nm.

2. Magnetic properties characterization

2.1.Hysteresis loop analysis

Figure 2(a) shows magnetichysteresis loops measured at 300K in the magnetic field applied in the planeof films grown at different oxygen pressures. The out-of-plane hysteresis loops (not shown here)have the reduced remnant magnetization (M_r/M_s) close to 0 thereby characterizing the hard magnetization axis for all the samples. This fact indicates that the films have easy plane magnetic anisotropy. It can be seenin (Fig.2(b)) that the coercive force (H_c) of the film grown at low oxygen pressure ($1\cdot10^{-6}$Torr) has the smallest value - 160 Oe. With increasing pressure up to $1.5\cdot10^{-6}$Torr, H_c reaches a maximum value of 369 Oe. However, with a subsequent increase in pressure to $3\cdot10^{-6}$Torr,H_c again decreases to 270 Oe and remains almost unchanged for the film with the (110) texture - 263 Oe, obtained at a higher pressure - $7\cdot10^{-6}$Torr. These values are close to the H_c values for polycrystalline Fe_3O_4 films grown on Si - 300 Oe for t = 80 nm (400°C) [30], 290 Oe for t = 100 nm (450°C) [31] and 275 Oe for t = 180 nm (350°C) [32].

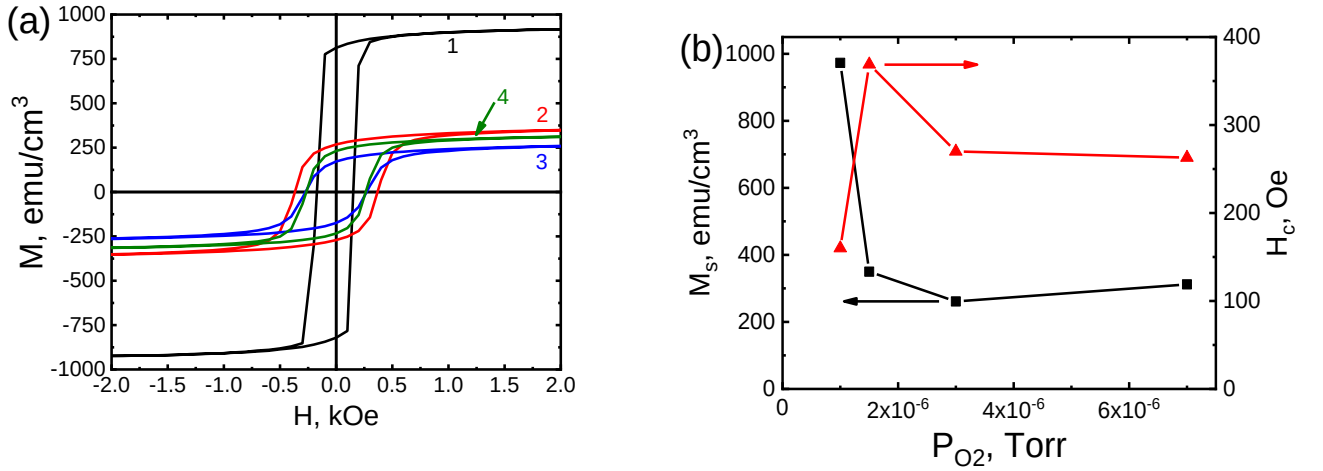

Fig.2.(a) In-plane magnetichysteresisloopsofthemagnetitefilmsgrownatP_{O2}: ***1***- $1\cdot10^{-6}$Torr, ***2***- $1.5\cdot10^{-6}$Torr, ***3*** - $3\cdot10^{-6}$Torrand***4*** - $7\cdot10^{-6}$Torr.(b) ThedependenceofM$_s$and$H_c$of the films as a function of the partial pressure of O_2.

The film grown at lowest oxygen pressure ($1\cdot10^{-6}$Torr) had the highest saturation magnetization M_s = 973 emu/cm^3. A higher M_s value than for bulk magnetite (M_{bulk}=471 emu/cm^3[33]), as well as a smallest value of the coercive force - 160 Oe, may be associated with the presence of non-oxidized iron in the film. As mentioned above, this is indirectly confirmed by the small film thickness - ~ 45 nm, not 75 nm as expected. The value of $M_s$sharply decreases with increasing oxygen pressure, Fig.2(b).The saturation magnetization reaches a minimum value of 261 emu/cm^{3}for a film with (311) texture grown at $P_{O2}=3\cdot10^{-6}$Torr. Although the H_c values for films with (110) and (311) textures practically did not differ, the M_s value for films with (110) texture ($P_{O2}=7\cdot10^{-6}$Torr) increased by 51 emu/cm^3 and reached to 312 emu/cm^3. This increase in M_s for a film with (110) texture is associated with an increase in the lateral dimensions of the Fe_3O_4 grains, as found from TEM data analysis. It can be noted that, for a Fe_3O_4 film grown at RT with a thickness of 80 nm and a grain size of ~ 13 nm, M_s did not exceed 200 emu/cm^3[29].

The magnetization is determined by the atomic structure and chemical composition of the nearest environment. The decrease in magnetization below the “bulk” value can be explained by defects at the boundaries between the crystallites. At the surface of magnetite nanocrystals, the spin-glass state [34,35] is usually realized with the magnetization close to zero. Thus, from the saturation magnetization one can estimate the volume fraction of disordered magnetite (magnetite in the spin-glass state) at the grain boundaries as:

$$v = 1 - M_s/M_{bulk} \quad (1)$$

The calculated values of ν are shown in Table 1. The defects level of the intercrystalline boundaries is various for different crystal textures. The data in Table 1 enables to observe how the texture and level of structural defects of a magnetite film (associated with grain boundaries) are correlated.

Table 1. Parameters of the studied samples.

Sample	P_{O2}, $1 \cdot 10^{-6}$Torr	texture	Grain size, nm	M_s, emu/cm^3	v	aH_a, kOe	H_R, kOe
1	1	no	33±6	973	-	0.494	2.69
2	1.5	(100)	55±6	350	0.18	1.19	4.44
3	3	(311)	22±3	261	0.37	1.203	3.74
4	7	(110)	49±5	312	0.27	1.037	3.76

2.2.Approach of the initial magnetization curves to magnetization saturation

The approach of the magnetization to saturation for the curves shown in Fig. 3 in the field range from 1 to 10 kOeis described by the following expression [36]:

$$M(H) = \chi \cdot H + M_s \cdot \left(1 - \frac{(aH_a)^2}{H^{(4-d)/2}\left(H^{d/2} + {H_R}^{d/2}\right)}\right) \quad (2)$$

where $H_R = 2 \cdot A/M_s \cdot {R_c}^2$, where H_R - the exchange field, A–the exchange stiffness, R_c – the correlation length of the local easy magnetization axis, H_a is the local magnetic anisotropy field of the volume with uniform orientation of the local easy axis of magnetization. It turned out that the best fit is achieved when the dimensionality$d$ = 3. The used values of H_R and aH_a are given in Table 1. Parameter$a = \sqrt{1/15}$for the uniaxial symmetry and$a = \sqrt{2/105}$for the cubic symmetry of the local magneticanisotropy for the textureless media.Depending on the sharpness of the texture this coefficient may vary from these values to zero[37]. In addition, for textureless samples, this coefficient would be between the uniaxial and the cubic values[38]. Since we do not have complete quantitative information on the texture and the relative contribution of the uniaxial and cubic components to the local magnetic anisotropy constant, in Table 1 we leave the productaH_a, which still allows us to judge the level of local magnetic anisotropy.

These data can be interpreted by making preliminary estimates for magnetite. Volumetric magnetite is characterized by cubic magnetic anisotropy with a negative constant of -1.3×10^5 erg/cm^3[39], the corresponding anisotropy field (540 Oe), saturation magnetization 471 emu/cm^3 and exchange constant 0.7×10^{-6} erg/cm^3. Using this data, the definition of $H_R = 2 \cdot A/M_s \cdot {R_c}^2$, and the magnitude of H_R from Table 1, we estimated the size of the localization region of the ordering of the local easy axis of magnetization R_c. This estimate gives the lengthR_c ~ 8-10 nm. The magnetic response is the sum of magnetization curves of small (~10 nm without texture) and large (~ 50 nm)crystallites. Large crystallites are magnetized to saturation in small fields, and small crystallites give that response in the field above 1 kOe, which is fitted by formula (2). Thus, in Table 1 we deal with the parameters of small crystallites. Their local anisotropy is higher than the anisotropy of bulk magnetite, since the surface contribution is already large. The three-dimensional nature of such a response is due to the fact that the small crystallite is exchange-coupled with large crystallites surrounding it from all sides.

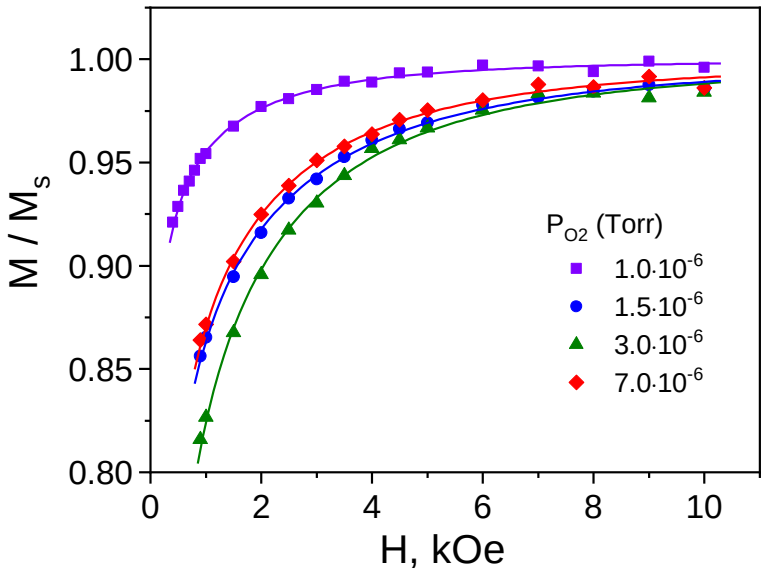

Fig.3. Approach of the magnetization to the saturation of films magnetized in the plane. Solid lines - fitting with equation (2).

2.3 FORC diagram analysis

The method of FORC diagrams [40-42] was used to analyze the magnetic behavior of the magnetite films with different microstructure. Unlike magnetic hysteresis loops, minor reversal curves named FORCs are usually used to analyze reversible and irreversible remagnetization processes and to visualize the interaction (H_u) and switching (H_c) fields distributions. A typical FORC diagram for a magnetic film can be built measuring a family of FORCs at various magnetic fields in the range from -5 to +5 kOe applied parallel and perpendicular to the film plane. First, a sample was saturated in the field H_s=5 kOe and then the field has been decreased to H_r. The magnetic moment m was measured in the field H, which was increasing from H_r to H_s with the step of 50 Oe. The FORC distribution $\rho(H, H_r)$ is defined as the family of mixed derivatives of the second order taken from $m(H, H_r)$:

$$\boldsymbol{\rho(H, H_r) = -\frac{1}{2}\left[\frac{\partial^2 m(H,H_r)}{\partial H \partial H_r}\right]} \quad (3)$$

We used a new set of coordinates (H_c, H_u), which were defined as $H_c = \frac{(H-H_r)}{2}$ and $H_u = \frac{(H+H_r)}{2}$.

The effect of the film texture on the distributions of H_c and H_u can be seen in Fig.4. The magnetite film without any texture has very narrow H_c- and H_u-distributions, Fig.4(a). Texture formation in the films deposited under higher O_2 pressure leads to the completely different FORC diagrams, Fig.4 (b-d). First of all, the distributions become significantly wider because of the larger variation of grain sizes. Second, the central peaks shifted relatively to H_c-axis to the negative area. Within the variable-variance moving Preisach model this asymmetry is due to that the effective field (H_{eff}) applied to the films can be considered as a sum of the externally applied field (H_{appl}) and a mean field (H_{mean}) proportional to the normalized magnetic moment of the sample [43,44]:

$$\vec{H} = \vec{H}_{appl} + \alpha \frac{\vec{m}}{\vec{m}_s}, \quad (1)$$

where α - proportionality constant (moving parameter), m_s – magnetic moment at saturation. As seen in Table 2, the values of H_{mean} are ranging from -30 to -63 Oe. The FORC diagrams have negative regions, which occurrence can be explained as a consequence of mean field interactions in the films [45].

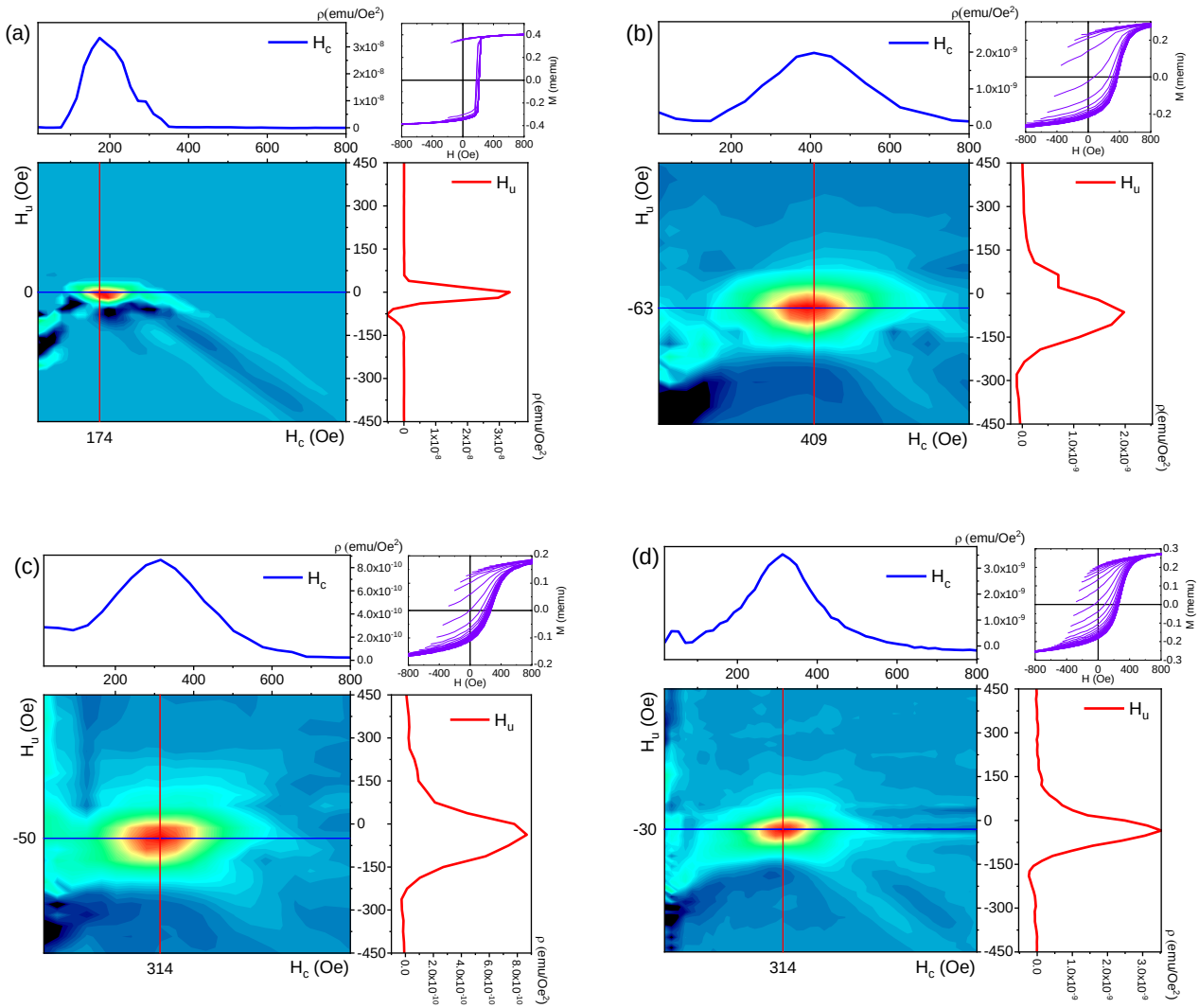

Fig.4. In-plane FORC diagrams of the magnetite films grown at P_{O2}: ***(a)***- $1 \cdot 10^{-6}$Torr, ***(b)***- $1.5 \cdot 10^{-6}$Torr, ***(c)*** - $3 \cdot 10^{-6}$Torr and ***(d)*** - $7 \cdot 10^{-6}$Torr. Each FORC diagram is accompanied with H_c- and H_u-profiles and family of FORCs.

As seen in Table 2, the peak values of H_c defined from FORC diagrams (H_c^{FORC}) corresponds closely to the measured major loop coercive force (H_c^{hyst}), but H_c^{FORC} is a little larger than H_c^{hyst} for all the films. This fact can be attributed to the influence of the mean-field demagnetizing interaction (H_{mean}), which is negative for samples 2, 3 and 4, Table 2. This means that in the textured films H_{mean} works against the external field trying to demagnetize the sample. The main reason for this is the exchange couplingbetween large and small crystallites, as is discussed in Section 2.2.The FORC diagram for the polycrystalline film (sample 1) has very narrow distributions of H_u and H_c (Fig.4a), which within the classical Preisach model corresponds to the switching of ideal square hysterons [45,46]. The small number of FORCs measured in the switching region between -180 to 180 Oe supports this conclusion. The formation of the crystal texture in the fully oxidized iron films drastically changes the FORC diagrams: the H_u and H_c distributions for samples 2-4 become much wider and the H_c- and H_u-profiles can be described by Gaussian function, Fig.4(b-d). The variation of the grain size in each film with the texture leads to the grain boundary density variation affecting the switching field distribution much strongly than that in the polycrystalline film.

Table 2. Magnetic parameters extracted from hysteresis loops and FORC diagrams.

Sample	H_c^{hyst}, Oe	H_c^{FORC}, Oe	ΔH_u, Oe	H_{mean}, Oe
1	168	174	25	0
2	362	409	80	-63
3	270	314	85	-50
4	263	314	48	-30

3. Magnetotransport properties

Figure 5 shows the dependence of the magnetoresistance on the magnitude of the applied external magnetic field (H) for Fe_3O_4 films grown on 1.5-nm-thick SiO_2/Si(001) at different oxygen pressures. The magnetoresistance (MR) was defined as MR=((ρ(H)-ρ_{max})/ρ_{max})×100%, where $\rho_{max}$is maximum value of resistivity atmagnetic field equal to the coercive force - $\rho_{max}=\rho(H_c)$.From Fig.5 it is clear that for all samples MR is negative and absolute valueincreases with the applied external field H. The largest values of MR ~ -2.2 and -2.5% correspond to Fe_3O_4 films with texture (311) and (110) grown at a pressure of $3\cdot10^{-6}$ and $7\cdot10^{-6}$ Torr.

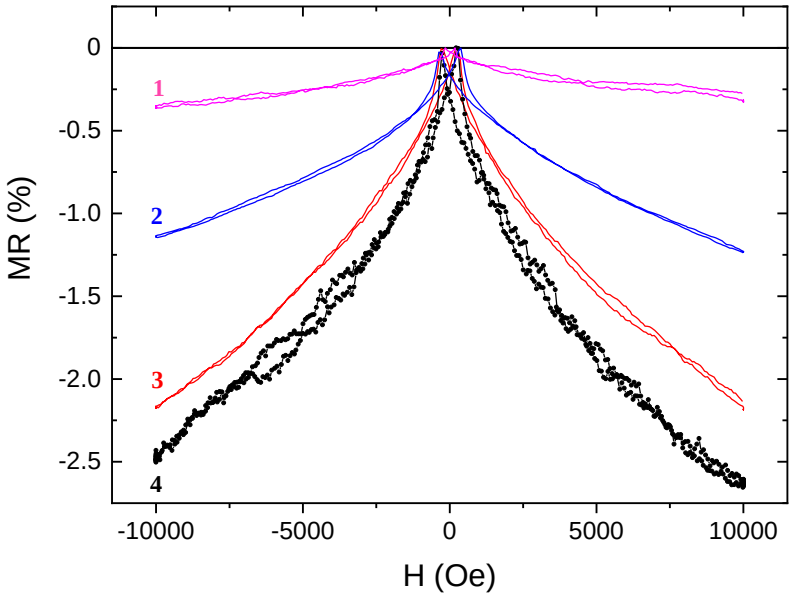

Fig.5. Magnetoresistance of the magnetite films grown on 1.5-nm-thick SiO_2/Si(001) at various P_{O2}: 1 – $1\cdot10^{-6}$ Torr, 2 – $1.5\cdot10^{-6}$ Torr, 3 – $3\cdot10^{-6}$ Torr, 4 –$7\cdot10^{-6}$ Torr.

An increase in MR for iron oxide films with increasing O_2 pressure was also observed in [27]. The maximum MR valuein Ref.[27] was obtained for a film grown at $5\cdot10^{-6}$ Torr, for which, according to Mössbauer spectrum, the phase composition corresponded exclusively to magnetite. The MR value for such a film was ~ -2% at H =10 kOe. The same MR value had a film deposited by magnetron sputtering at RT[28]. As in [27], smaller MR values for films grown at low pressures ($1\cdot10^{-6}$ Torrand $1.5\cdot10^{-6}$ Torr) are explained by the presence of the paramagnetic phase FeO, the Debye ring from which we observed by RHEED during film growth [23]. In contrast to the Fe_3O_4 film deposited at RT in [27], the films in this work were grown on a hot substrate (T_{sub}=300°C) and had (311) and (110) textures.

In Ref.[47], the MR value for a 500-nm-thick polycrystalline film withthe (110) texture grown on a Si substrate was -1.7% at H = 0.5 T (5 kOe). This MR value is close to ~ -1.8% for a film with the same texture grown in this work (curve 4 in Figure 5), although the grain size in the aforementioned

work was 1-2 μm, and in the present work it did not exceed 50 nm.In the case of 50-nm-thick films with the (111) texture, the MR value was ~ 1.6% for H = 1 T [11], which is almost 1% less than for a film with the (110) texture grown in this work.

It is assumed that the magnetoresistance is associated with the presence of APBs in the defective places of the Fe_3O_4 film, which have packaging defects in the crystal lattice with a spinel structure. It has been shown that in epitaxial Fe_3O_4 films a change in the density of APBs leads to a change in their conductivity [48] and magnetoresistance [49]. APBs influence (act as a barrier) on electron transport due to the presence of strong antiferromagnetic spin interaction on them. Under the influence of an external magnetic field (H), spin ordering occurs on APBs, as a result of which, the barrier height for electrons tunneling through APBs decreases, and the film conductivity increases [50]. In this case, reducing the resistance of the film in the field H causes negative MR values. In the case of polycrystalline films, grain boundaries and stoichiometry near them should be taken into account.The authors of the works [51] and [51] note that magnetoresistance due to spin-dependent scattering within grain boundary (GB) is similar to the case of epitaxial Fe_3O_4 films showing magnetoresistance attributed to scattering at APBs.Since the presence of APBs was observed inside the grains[32], the MR value for polycrystalline films should depend on the spin-dependent scattering within both GBs and APBs.

The resistivity of films without texture and with (100) texture grown at low oxygen pressure was 0.045 and 1.45 mOm·cm, that is significantly less than 4 mOm·cm for bulk magnetite [52]. The higher conductivity of the films can be explained by the presence of non-oxidized iron, the existence of which, as mentioned above, was also indicated by the analysis of magnetic hysteresis loops. In contrast, the resistivity values for magnetite films with (311) and (110) textures were higher than 4 mOm·— 0.184 and 0.129 Om·cm.These values are smaller than the values of 0.22 Om·cm [27] and ~ 0.7 Om·cm [29] for magnetite films without a texture with thickness of 75 and 80 nm grown at a low temperature (~ 300 K). It was noted [27, 29] that the value of resistivity strongly depends on the grain size and density of grain boundariesin polycrystalline films.In contrast to the films obtained in this work, the higher resistivity of “low temperature” films with a grain size of ~ 13 nm [29] can be explained by the higher density of grain boundaries.Larger grains in the case of a film with (110) texture may explain the reduction in resistivity by 30% compared to a film with (311) texture.

Conclusions

Using the method of reactive deposition of iron in an oxygen atmosphere, polycrystalline iron oxide films were grown on the surface of a Si(001) substrate with an ultrathin SiO_2 layer. The structural, electrical, and magnetic properties of the films were studied as a function of the oxygen partial pressure. It has been defined that pressure affects not only the phase composition of the films, but also the orientation of the Fe_3O_4 grains formed in them. Starting with a pressure of $3 \cdot 10^{-6}$Torr, the grown film consisted only of magnetite grains with thepreferred (311) orientation, and at a higher pressure — with the (110) orientation. An analysis of magnetic and electrical data showed that a film with the (110) texture has a higher saturation magnetization and a lower resistivity compared to a film having the (311) texture. This result is proposed to explain the increase in the size of magnetite grains with oxygen pressure. It has been found that a magnetite film with the (110) texture had a higher magnetoresistance value than films grown at low oxygen pressures.The approach to magnetization saturation in combination with the FORC diagram method proved the existence of the exchange coupling between large and small grains.

Acknowledgments

This work is supported in part by the Russian Ministry of Education and Science under the state tasks (3.5178.2017/8.9 and 3.4956.2017), by Act 211 of the Government of the Russian Federation (contract

No. 02.A03.21.0011)and by the Comprehensive Program of Basic Research of the FarEastern Branch of the Russian Academy of Sciences "Far East" 2018−2020 № 18-3-022 (0226-18-0031).

References

[1] M. Fonin, Y. Dedkov, C. König, G. Güntherodt, U. Rüdiger, J. Mayer, D. Vyalikh, and S. Molodtsov, in *Advances in Solid State Physics*, edited by B. Kramer (Springer Berlin Heidelberg, Berlin, Heidelberg, 2003), pp. 487.
[2] G. Zhang, C. Fan, L. Pan, F. Wang, P. Wu, H. Qiu, Y. Gu, and Y. Zhang, J Magn Magn Mater **293**, 737 (2005).
[3] A. M. Bataille, L. Ponson, S. Gota, L. Barbier, D. Bonamy, M. Gautier-Soyer, C. Gatel, and E. Snoeck, Phys Rev B **74**, 155438 (2006).
[4] M. Fonin, Y. S. Dedkov, R. Pentcheva, U. Rüdiger, and G. Güntherodt, Journal of Physics: Condensed Matter **19**, 315217 (2007).
[5] R. Prakash, R. J. Choudhary, L. S. Sharath Chandra, N. Lakshmi, and D. M. Phase, Journal of Physics: Condensed Matter **19**, 486212 (2007).
[6] S. K. Arora, H. Wu, H. Yao, W. Y. Ching, R. J. Choudhary, I. V. Shvets, and O. N. Mryasov, Ieee T Magn **44**, 2628 (2008).
[7] X. Huang and J. Ding, Journal of the Korean Physical Society **62**, 2228 (2013).
[8] M. Imran, A. Akbar, S. Riaz, S. Atiq, and S. Naseem, Journal of Electronic Materials **47**, 6613 (2018).
[9] A. S. Samardak, A. V. Davydenko, A. V. Ognev, Y. S. Jeon, Y. S. Choi, and Y. K. Kim, Jpn J Appl Phys **55**, 100303 (2016).
[10] Z. Zhang and S. Satpathy, Phys Rev B **44**, 13319 (1991).
[11] E. Liu, Y. Yin, L. Sun, Y. Zhai, J. Du, F. Xu, and H. Zhai, Appl Phys Lett **110**, 142402 (2017).
[12] B. T. Jonker, Proceedings of the IEEE **91**, 727 (2003).
[13] G. Schmidt, Journal of Physics D: Applied Physics **38**, R107 (2005).
[14] M. Bohra, N. Venkataramani, S. Prasad, N. Kumar, D. S. Misra, S. C. Sahoo, and R. Krishnan, J Magn Magn Mater **310**, 2242 (2007).
[15] J.-G. Yun, Y.-M. Lee, W.-J. Lee, C.-S. Kim, and S.-G. Yoon, Journal of Materials Chemistry C **1**, 1977 (2013).
[16] S. P. Sena, R. A. Lindley, H. J. Blythe, C. Sauer, M. Al-Kafarji, and G. A. Gehring, J Magn Magn Mater **176**, 111 (1997).
[17] E. Aubry, T. Liu, A. Dekens, F. Perry, S. Mangin, T. Hauet, and A. Billard, Materials Chemistry and Physics **223**, 360 (2019).
[18] H. Yanagihara, M. Myoka, D. Isaka, T. Niizeki, K. Mibu, and E. Kita, Journal of Physics D: Applied Physics **46**, 175004 (2013).
[19] J. Zhang *et al.*, J Magn Magn Mater **432**, 472 (2017).
[20] S. K. Singh, S. Husain, A. Kumar, and S. Chaudhary, J Magn Magn Mater **448**, 303 (2018).
[21] C. Schönenberger, S. F. Alvarado, and C. Ortiz, J Appl Phys **66**, 4258 (1989).
[22] Y. K. Kim and M. Oliveria, J Appl Phys **75**, 431 (1994).
[23] V. V. Balashev, V. A. Vikulov, T. A. Pisarenko, and V. V. Korobtsov, Phys Solid State+ **57**, 2532 (2015).
[24] C.-H. Lai, P.-H. Huang, Y.-J. Wang, and R. T. Huang, J Appl Phys **95**, 7222 (2004).
[25] V. V. Balashev, V. V. Korobtsov, T. A. Pisarenko, and L. A. Chebotkevich, Technical Physics **56**, 1501 (2011).
[26] P. B. Barna and M. S. Adamik, in *Science and Technology of Thin Films* (WORLD SCIENTIFIC, 1995), pp. 1.
[27] T. Furubayashi, J Appl Phys **93**, 8026 (2003).
[28] W. B. Mi, H. Liu, Z. Q. Li, P. Wu, E. Y. Jiang, and H. L. Bai, Journal of Physics D: Applied Physics **39**, 5109 (2006).
[29] H. Liu, E. Y. Jiang, H. L. Bai, R. K. Zheng, and X. X. Zhang, Journal of Physics D: Applied Physics **36**, 2950 (2003).
[30] C. Boothman, A. M. Sánchez, and S. van Dijken, J Appl Phys **101**, 123903 (2007).
[31] R. J. Kennedy and P. A. Stampe, J Magn Magn Mater **195**, 284 (1999).

[32] J. Tang, K.-Y. Wang, and W. Zhou, J Appl Phys **89**, 7690 (2001).
[33] *Magnetic and Other Properties of Oxides and Related Compounds · Part B* (Springer-Verlag, Berlin, 1970), Vol. 4B.
[34] R. H. Kodama, J Magn Magn Mater **200**, 359 (1999).
[35] A. P. Safronov, I. V. Beketov, S. V. Komogortsev, G. V. Kurlyandskaya, A. I. Medvedev, D. V. Leiman, A. Larrañaga, and S. M. Bhagat, AIP Advances **3**, 052135 (2013).
[36] S. V. Komogortsev and R. S. Iskhakov, J Magn Magn Mater **440**, 213 (2017).
[37] R. S. Iskhakov, S. V. Komogortsev, A. D. Balaev, and L. A. Chekanova, Journal of Experimental and Theoretical Physics Letters **72**, 304 (2000).
[38] S. V. Komogortsev, S. I. Smirnov, N. A. Momot, and R. S. Iskhakov, Journal of Siberian Federal University. Mathematics & Physics **3**, 515 (2010).
[39] J. M. D. Coey, *Magnetism and Magnetic Materials* (Cambridge University Press, Cambridge, 2010).
[40] I. Mayergoyz, Ieee T Magn **22**, 603 (1986).
[41] C.-I. Dobrotă and A. Stancu, J Appl Phys **113**, 043928 (2013).
[42] Y. Cao, K. Xu, W. Jiang, T. Droubay, P. Ramuhalli, D. Edwards, B. R. Johnson, and J. McCloy, J Magn Magn Mater **395**, 361 (2015).
[43] P. Postolache, M. Cerchez, L. Stoleriu, and A. Stancu, Ieee T Magn **39**, 2531 (2003).
[44] A. S. Samardak *et al.*, Journal of Alloys and Compounds **732**, 683 (2018).
[45] A. Stancu, C. Pike, L. Stoleriu, P. Postolache, and D. Cimpoesu, J Appl Phys **93**, 6620 (2003).
[46] F. Preisach, Zeitschrift für Physik **94**, 277 (1935).
[47] J. M. D. Coey, A. E. Berkowitz, L. Balcells, F. F. Putris, and F. T. Parker, Appl Phys Lett **72**, 734 (1998).
[48] W. Eerenstein, T. T. M. Palstra, T. Hibma, and S. Celotto, Phys Rev B **66**, 201101 (2002).
[49] A. V. Ramos, J. B. Moussy, M. J. Guittet, A. M. Bataille, M. Gautier-Soyer, M. Viret, C. Gatel, P. Bayle-Guillemaud, and E. Snoeck, J Appl Phys **100**, 103902 (2006).
[50] P. Li, L. T. Zhang, W. B. Mi, E. Y. Jiang, and H. L. Bai, J Appl Phys **106**, 033908 (2009).
[51] X. Liu, W. Mi, Q. Zhang, and X. Zhang, Appl Phys Lett **113**, 012401 (2018).
[52] P. A. Miles, W. B. Westphal, and A. Von Hippel, Reviews of Modern Physics **29**, 279 (1957).